Composites Part B 79 (2015) 595–603

Contents lists available at ScienceDirect

Composites Part B

journal homepage: www.elsevier.com/locate/compositesb

Tribo-mechanical characterization of reinforced epoxy resin under dry and lubricated contact conditions

Alessandro Ruggiero [a], Massimiliano Merola [a, *], Pierpaolo Carlone [a], Vasiliki-Maria Archodoulaki [b]

[a] Department of Industrial Engineering, University of Salerno, Via Giovanni Paolo II 132, 84084 Fisciano SA, Italy
[b] Institute of Materials Science and Technology, Vienna University of Technology, Favoritenstrasse 9-11, A-1040 Vienna, Austria

ARTICLE INFO

Article history:
Received 11 February 2015
Received in revised form
13 April 2015
Accepted 9 May 2015
Available online 16 May 2015

Keywords:
A. Polymer-matrix composites (PMCs)
B. Porosity
B. Mechanical properties
B. Wear

ABSTRACT

The aim of the present work is to investigate the influence of the reinforcing material and architecture on the voids content, mechanical properties and tribological behavior of fiber reinforced epoxy composite laminates manufactured by VARTM under different processing conditions. Two different textile architectures, namely unidirectional non-crimp fabrics (UD) and 0/90 plain wave (PW), were considered, reinforcing an EPIKOTE RIMR 135 epoxy matrix with glass (GF) as well as carbon (CF) continuous fibers. Optical observations revealed an unexpected trend relatively to the intra- and inter-bundle voids concentration with respect to the impregnation velocity, especially using UD-CF and UD-GF reinforcements and low impregnation rate. Tensile and three points bending tests highlighted the dominant role of fiber material and architecture on mechanical properties, whereas the presence of voids played a minor role with respect to the analyzed features. Tribological outcomes evidenced a reduction of the friction coefficient (μ) when the resin is reinforced by carbon or glass fibers. The lowest values were detected when the sliding direction of the counterbody is oriented parallel to the fiber direction for UD samples. Further reduction of μ, for both UD and PW specimens, was obtained by interposing a lubricant at the interface.

1. Introduction

Fiber Reinforced Polymer (FRP) are widely used in applications with interacting surfaces in relative motion such as seals, gears and dry slide bearing materials1 [1–3], as well as orthopaedic prostheses [4]. In this context, determining the mechanical and tribological behavior of involved components is a key factor. Carbon and glass are two of the most widespread fiber reinforcements for epoxy resin. Increasing compressive and shear strength of the resin, fibers support part of the applied load and lower the wear rate. Nevertheless, the understanding of tribological properties of glass and carbon fiber reinforced polymer is still"limited and lacks predictability" [5].

In recent years, Liquid Composite Molding (LCM) processes, such as Vacuum Assisted Resin Transfer Molding (VARTM), have gained a lot of attention in composite manufacturing. Main advantages of LCM processes are related to the capability of manufacturing geometrically complex products with remarkable precision, flexibility of reinforcement architecture and reduced human exposure to dangerous emission of volatiles. VARTM is a multi-step process defined by preform impregnation, resin cure and eventually post-cure.

During VARTM process, a multiphase flow, i.e. resin and air bubbles, moves inside the fiber preform. The combination of multiples factors, such as temperature, pressure and fluid viscosity, could lead to void formation. It is well established that these voids negatively affect the final mechanical properties. Ghiorse discussed that the interlaminar shear strength and flexural strength of carbon fiber/epoxy composites decrease by 10% and the flexural modulus decreases by 5% for each 1% void content increase in the range 0%–5% [6].

Two kinds of voids are generally observed in a composite manufactured by LCM process. A dual-scale porosity and void content can be defined and characterized measuring the intra-bundle micro-voids and the inter-bundle macro-voids. Patel and Lee [7,8] described the alternation of macro- and micro-voids, attributable to two different flow dynamics. Indeed, at low impregnation rates, due to predominant capillary pressure, the

* Corresponding author.
E-mail addresses: ruggiero@unisa.it (A. Ruggiero), mmerola@unisa.it (M. Merola), pcarlone@unisa.it (P. Carlone), vasiliki-maria.archodoulaki@tuwien.ac.at (V.-M. Archodoulaki).

http://dx.doi.org/10.1016/j.compositesb.2015.05.015
1359-8368/

resin flows faster inside the tows than between them. Therefore, when the resin creates a cross flow, macro void could take place in the empty gap. When the flow rate is high, viscous forces are consequently elevate and rule the flow, yielding micro-voids formation and unsaturated spots. Other researchers, including Labat et al. [9] demonstrated that the percentage of macro/micro-voids formation is a near logarithmic function of the fluid flow velocity: macro-voids decrease with velocity whereas micro-voids increase. It is so possible, in theory, to estimate the optimal infiltration velocity that minimizes the void ratio. This phenomenology is currently subject of an amply debate, as documented in several reports dealing with void content prediction and monitoring [7–10].

As tribological loaded components, the coefficient of friction, wear rate and stress carrying capacity are materials key factors. The behavior of the contact zones during relative movements is influenced by properties of resin, fiber and their interface. Some tribological studies were carried out on fiber reinforced epoxy in dry condition with constant sliding velocity [5,11–14]. Their results showed how the presence of fibers with good tribological characteristics leads to a lower value of the coefficient of friction and a lower wear rate. Lancaster [11] argued the enhancement of the wear resistance of a polymer matrix through the mean of carbon fibers, for they support part of the load applied to the sample. Larsen et al. [5] found a μ decrease of 35% by substituting a glass fiber weave with a carbon/aramid hybrid weave in epoxy-matrix. Many of these works highlighted a strong correlation between the sliding direction and the orientation of unidirectional fibers. A low wear rate, around 10^{-16} m^3 N^{-1} m^{-1}, along with low μ (0.2) was observed by Sharma et al. [15] for CF/polyetherimide composites with reinforcement parallel to load direction. Kim et al. [16] found that the friction and wear behavior of PA12 composite samples were more dependent on the fiber ratio than on the sliding direction, reaching the lowest μ at 30wt.% of glass fiber.

As debated in Refs. [15,17–19], a continually reversing load applied by the moving counterbody has a strong influence on the friction and wear behavior. Schön [17] measured the μ for composite in contact with composite in reciprocal sliding in order to model bolted joints of CF/epoxy material, founding a starting value of 0.65 and a peak of 0.74. Klingshirn et al. [18] investigated the influence of the volume content of short carbon fibers inside an epoxy matrix on the fretting wear rate, demonstrating the dramatically decrease of this parameter with a growing fiber content.

To authors best knowledge, studies on the different tribobehavior of FRP in dry and lubricated conditions during reciprocating sliding have not yet been reported. Since in many mechanical applications this kind of materials are used in reciprocating movement, a more complete tribological investigation is necessary.

The aim of this study is to investigate both mechanical and tribological behavior of GF and CF reinforced epoxy, taking into account the influence of the production parameters on the laminates voids content. The observation by Patel and Lee [7,8] was experimentally checked, by means of a thermogravimetric analysis (TGA) and microscopic observations. Tensile and bending tests were executed to find a quantitative correlation between voids and mechanical properties. From a tribological point of view the system here analyzed consists in FRP laminate coupled with steel (AISI E52100) in dry and lubricated conditions under reciprocating motion.

2. Materials and methods

Composite laminates were manufactured by VARTM, reinforcing an epoxy matrix with glass (GF) or carbon (CF) continuous fibers. Reinforcing fibers were organized following two different textile architecture, namely unidirectional non-crimp fabrics (UD) and plain-weave (PW). EPIKOTE RIMR 135 mixed with EPIKURE curing agent RIMH 137, manufactured by Momentive, was employed as epoxy system. Glass fibers were boron-free E-CR from Advantex. Carbon fibers were high tenacity HTA40 from Tenax. Mechanical and physical properties of used constituents are listed in Table 1.

Four layers of reinforcement were piled in the center of the mold, lied on a release agent and covered by the peel-ply and the distribution media for each processing condition. Afterward the vacuum bag was placed on top and sealed on the mold. The impregnation rate was varied regulating the applied vacuum pressure, considering three level (500, 800 and 950 mbar) for this process variable. In Fig. 1 the experimental setup is shown, along with a schematic representation of the final laminates.

Infusion step was monitored by means of a video-camera. In Table 2 is reported the time that the resin took going from the inlet to the outlet hoses. Laminates were demolded after 24 h of cure at room temperature.

A first estimation of the void concentration was obtained by the TGA, performed using a Mettler Toledo TGA/DSC1. TGA outcomes were post-processed using the following equation, derived in Ref. [20]:

$$V_v = \frac{\rho_c^0 - \rho_c}{\rho_c^0} \tag{1}$$

being V_V the void volume ratio, ρ_c^0 is the density of the composite in the absence of voids as provided by the TGA analysis, and ρ_c the mean density measured by immersion on three specimens for each kind of plate.

Observations of the laminate cross and longitudinal sections (along plane 2–3 and 1–3, respectively) were made on a Zeiss Axioplan optical microscope. Rough grinding and polishing of specimens were previously made on a Struers Tegra Doser-5. Voids are easily identifiable as the darkest spots on the micrographs. An image processing and analysis routine was implemented to identify and measure the extension of voids. Then, void area fraction was inferred by dividing the cumulative area of detected voids by the total area of the images. Finally void volume fraction was obtained averaging the area fraction on ten different measurements.

Tensile tests were performed with reference to ISO 527-4. Four straight-sided specimens were prepared for each laminate. Specimens were cut along axis 1 (Fig. 1a,b) for both UD and PW laminates. Tensile specimens were cut with the dimensions of 250 × 25 × 1 mm^3, following the standard's prescriptions. To characterize the laminates under flexural conditions a three-point-bending test was used, as specified by the ISO 14125 standard. Four specimens per laminate were made, with dimensions 40 × 15 × 1 mm^3 and 20 × 15 × 1 mm^3 for carbon and glass fiber reinforced laminates, respectively. Cutting orientations were the same as tensile specimens.

Tribotests were executed on a Ducom Reciprocatory Friction Monitor with ball-on-flat configuration. This apparatus analyzes the tribological behavior of tribopairs: a flat material in contact

Table 1
Mechanical and physical proprieties of fibers and matrix.

	Density (g cm^{-1})	Tensile strength (MPa)	Modulus of elasticity (GPa)
Epoxy resin	1.18–1.20	60–75	2.7–3.2
Carbon fiber	1.76	3950	238
Glass fiber	2.26	3100–3800	80–81

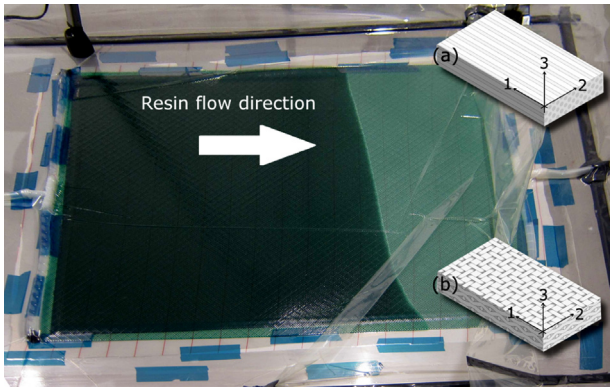

Fig. 1. The VARTM process and representation of (a) unidirectional and (b) plain weave laminae.

Table 2
Laminates codenames and impregnation time.

Fiber material	Textile architecture	Vacuum pressure (mbar)	Codename	Impregnation time (s)
Carbon	Plain weave 0/90	950	CF_PW_950	150
		800	CF_PW_800	195
		500	CF_PW_500	360
	Unidirectional	950	CF_UD_950	175
		800	CF_UD_800	200
		500	CF_UD_500	230
Glass	Plain weave 0/90	950	GF_PW_950	230
		800	GF_PW_800	345
		500	GF_PW_500	370
	Unidirectional	950	GF_UD_950	45
		800	GF_UD_800	95
		500	GF_UD_500	160

with an alternative moving counterbody (see Fig. 2). The tests parameters were chosen considering the work by Dhieb [21]. The counterpart selected was a common steel (AISI E52100) sphere of 10 mm in diameter. The ball rubbed against the FRP specimens under an applied normal load of 9 N realizing a mean contact pressure of 262 MPa. The latter parameter was evaluated using the Hertzian contact theory, considering that the first layer of the specimens is always epoxy resin, for both CF and GF reinforced laminates, therefore this value is considered a good approximation during the initial rubbing phase. A linear actuator alternatively moved the sphere at an harmonic alternative motion, with frequency of 6 Hz. Stroke length was 1 mm and test duration was setted to 200 min. For the plain weave samples the stroke length was increased to 3 mm, to assure the sliding on both warp and weft

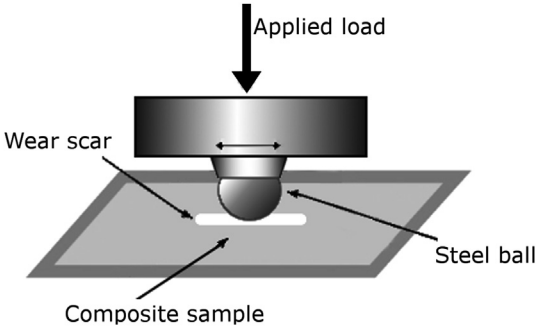

Fig. 2. A schematic representation of the tribotest.

Table 3
Tests parameters.

Test	Number*	Specimen main properties	
		CF	GF
TGA	3	700 ± 20 (mg)	800 ± 20 (mg)
Tensile	4	250 × 25250 × 1 (mm^3)	250 × 25 × 1 (mm^3)
Three points bending	4	40 × 15 &times 1 (mm^3)	20 × 15 × 1 (mm^3)
Tribotest	5	10 × 25 × 6 (mm^3)	10 × 25 × 6 (mm^3)

*Number of specimens for each reinforced laminate typology.

directions of the fiber texture. In the case of the UD FRP, sliding direction was parallel (along axis 1 in Fig. 1a) and anti-parallel (axis 2 in the same figure). Before each test, the specimen and the counterbody were cleaned using ethanol. Lubricated tribotests were carried out by using ETRO4 (group III base oil) as lubricant between the steel counterpart and the laminate. Every test was realized in room temperature, in laboratory air at controlled levels of relative humidity. For each specimens at least five tests were carried out, averaging the final results. In order to investigate on the wear phenomena [22–24] and on the possibility that a lubrication mechanism took place during the tribotests, a first qualitative topographic analysis was executed. The analysis was carried on by using a Sensofar PLu neox 3D optical profiler. After each test, the worn surfaces were cleaned with ethanol, to remove debris, and then scanned with a 20x confocal brightfield objective. The sensor head moved along the Z-axes (orthogonal to the specimen surface) with a mean stroke of 40 μm, using steps of 1 μm. This yielded detailed 3D scans of the specimens in the wear scars.

A summary of the different tests executed on the samples is shown in Table 3.

3. Results and discussion

TGA outcomes, i.e. weight and volume fractions of fiber, matrix and voids are presented in Table 4. In particular, resin and fiber weight fractions are indicated, respectively, as W_r and W_f, whereas V_r and V_f indicate the corresponding volume fractions. V_v is the estimation of the void content obtained by means of Equation (1). Whereas V_v^i is the void volume ratio calculated by image analysis. The uncertainty in density measurement yielded to some unrealistic values of V_v (almost null in the negative side). These values were not reported in the table and the parameter was assumed equal to zero.

In Fig. 3 some sample images, provided by the microscopic analysis, are shown. As can be seen, porosity appears as the darker areas, whereas the matrix can be distinguished by its brighter contrast and smoother surface. Fibers are the brightest elements observed. In longitudinal samples cut parallel to fiber direction,

Table 4
Resin, fiber and void fractions.

Codename	W_r %	W_f %	ρ_c^0 (g cm^3)	V_r %	V_f %	ρ_c (g cm^3)	V_v %	V_v^i %
CF_UD_500	45.73	46.53	1.5	60.49	39.59	1.37	8.8	6.10
CF_UD_800	42.48	51.2	1.5	56.34	43.68	1.41	6.27	5.96
CF_UD_950	45.96	48.08	1.47	59.78	40.22	1.44	2.28	0
CF_PW_500	46.81	53.05	1.4	57.84	42.16	1.42	–	0.74
CF_PW_800	47.55	52.39	1.39	58.53	41.47	1.41	–	0
CF_PW_950	48.84	51.03	1.39	59.81	40.19	1.41	–	0
GF_UD_500	48.35	51.65	1.63	66.56	33.44	1.61	–	1.3
GF_UD_800	47.85	52.15	1.63	66.25	33.75	1.64	–	0
GF_UD_950	48.35	51.65	1.64	65.81	34.2	1.62	–	0
GF_PW_500	46.23	53.77	1.6	68.42	31.58	1.64	–	0
GF_PW_800	45.9	54.1	1.61	67.99	32.02	1.65	–	0
GF_PW_950	45.4	54.6	1.6	68.42	31.58	1.64	–	0

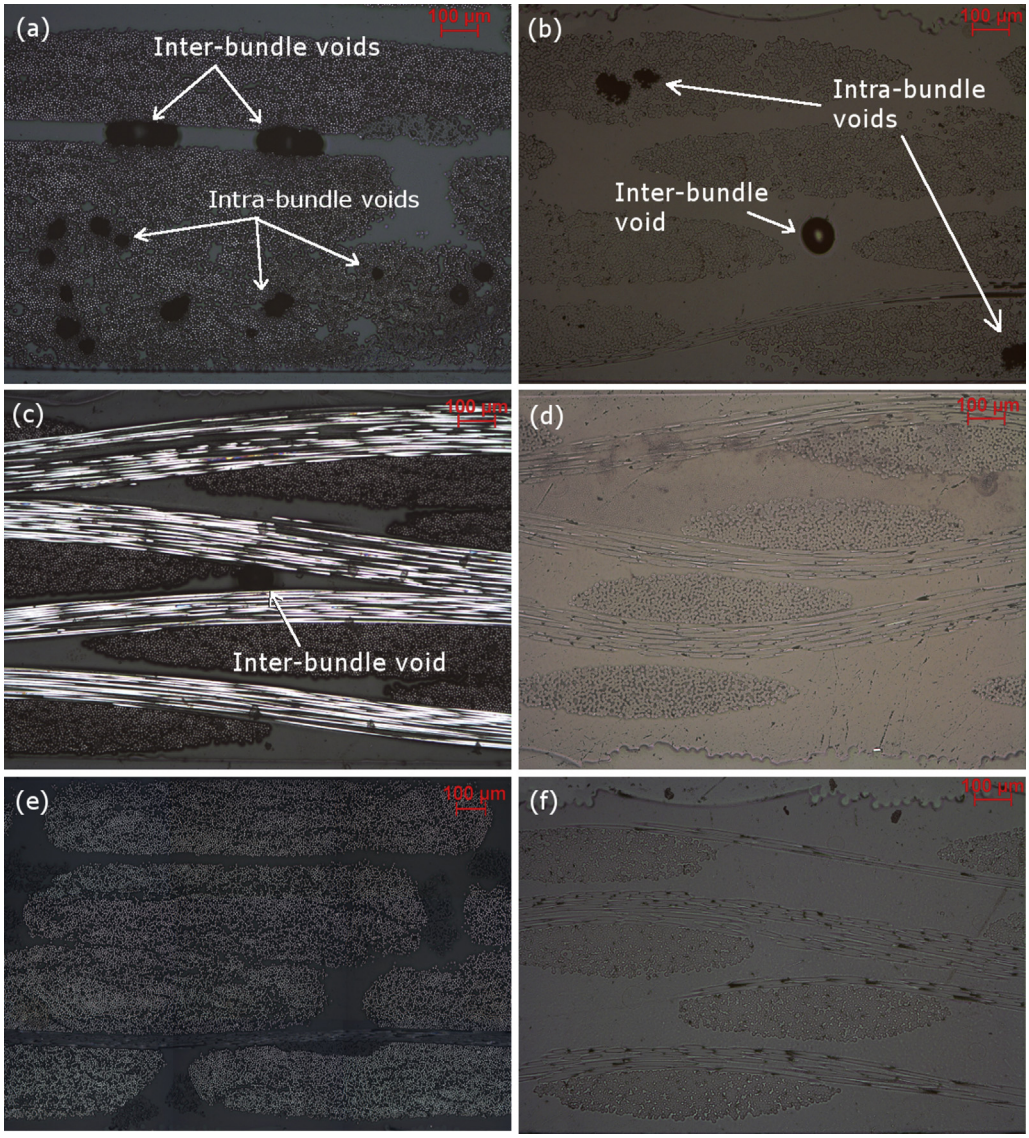

Fig. 3. Micrographs of some specimen sections. The first three: (a) CF_UD_500, (b) GF_UD_500 and (c) CF_PW_500 evidence the presence of voids. In (d) GF_PW_500, (e) CF_UD_950 and (f) GF_PW_500 no voids are detected.

fibers appear as elongated sections, whereas in cross-section samples, they exhibit circular or ellipsoidal shapes. Microscopic observations revealed simultaneous presence of both inter- and intra-bundle pores. This concurrent condition was more evident in the UD-CF samples obtained adopting the lowest considered vacuum pressure, i.e. promoting lowest impregnation velocity.

As the vacuum pressure increased, and therefore the impregnation velocity rose, the concentration of both kind of voids receded. The image analysis algorithm provided also void volume ratios. Nevertheless, small regions of damaged fibers (broken during polishing) exhibit similar contrast, and may lead to wrong results. For this reason, the brightness threshold routine was enhanced applying a morphological algorithm. The results are reported in the last column of Table 4. In UD-CF plates there was a sensible increase of the void ratio when impregnation was slower. In these samples, lowering from 950 mbar to 800 mbar of vacuum pressure leaded a 6% of void ratio increase. PW-CF laminates were sensibly less affected by voids generation. Therefore, the different textile architecture, which corresponds to a different wettability, affected the void creation and concentration during the infusion process. Regarding the GF laminates, only the UD samples presented void content different from zero, being V_v equal to 1.3% at the highest impregnation time (160 s). In the other specimens, it was not found any relevant presence of voids. This conclusion, which is adequately congruent with TGA void volume ratio prediction, find again its explanation in the different wettability and geometry of fiber constituents.

Figs. 4 and 5 present the tensile test results with positive standard deviation bars for each processing condition. Obtained outcomes did not point out a well-defined relation between tensile properties and impregnation velocity (or vacuum pressure). It is possible to notice a small increase in modulus and strength when the pressure moved from 500 to 800 or even 950 mbar. As previously noticed, the most evident presence of voids was found in UD-CF, for this reason a particular attention was dedicated on these samples, to find a correlation between voids and mechanical properties. In these samples an increasing strength was found, as the vacuum pressure raised; however, not the same positive trend is noticeable for the modulus of elasticity. In conclusion, it is not possible assure better behaviors in term of tensile response as the

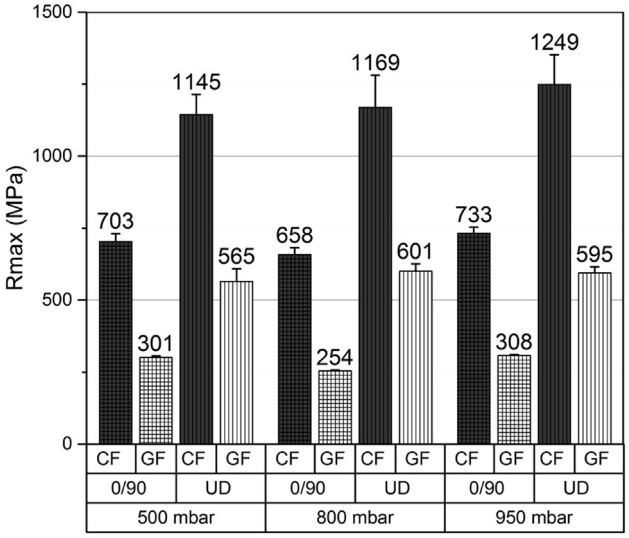

Fig. 4. Ultimate tensile strength.

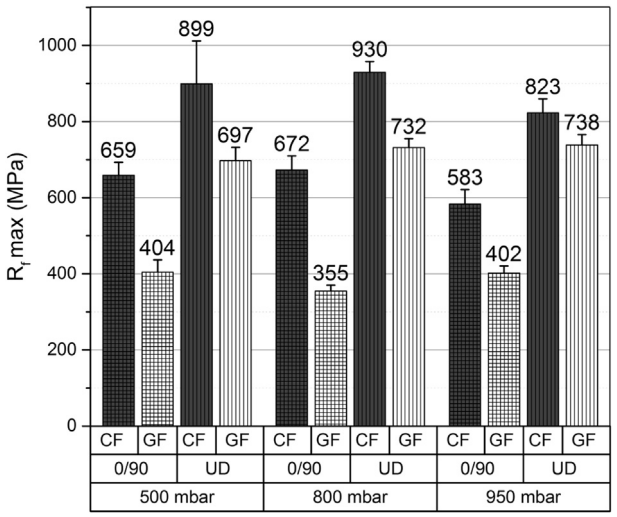

Fig. 6. Ultimate flexural strength.

V_v decreased in UD-CF. Such a result was expected, since in literature is confirmed that fiber-dominated mechanical properties are not significantly influenced by voids [25].

Likewise tensile, also bending experiments highlighted the influence of the reinforcement on mechanical properties of the laminates. It was not possible to find a specific trend of the bending properties with different vacuum pressures. As showed in Figs. 6 and 7 a better response to bending was likely to be obtained with an infusion pressure higher than 500 mbar. During the tests, it has been noticed an unusual behavior of the UD-CF, an earlier fracture occurred for the samples obtained with 950 mbar. The mean ultimate stress value decreases for both UD and PW.

Regarding tribological tests, the kinetic friction coefficient (μ), measured by the piezoelectric transducer, exhibited the expected behavior for each specimens analyzed in dry test conditions [26]. Due to the large amount of the obtained data, only an exemplificative behavior of μ obtained during the first testing hour is reported in Fig. 8. At the beginning of the test the μ was reached its maximum values; this is attributable to a first contact between the steel sphere and the epoxy resin (this tribopair has a μ of approximately 0.9). Once this layer was removed the fibers were exposed and the μ decreased. As can be seen, the bulk epoxy resin exhibited an increasing μ, whereas both the glass and the carbon fiber laminates showed a slow decreasing trend after the initial peak, giving a μ in the range of 0.4–0.7 which kept lowering. The μ curve of CF parallel and anti-parallel specimens had a much more rapid decrease than the GF.

The final μ was evaluated by averaging the last 10,000 data points (17 min) of the complete test. The final mean values of μ in dry conditions for the reinforced laminates are reported in Fig. 9. From these results it is possible to conclude that the lowest μ was obtained in case of parallel sliding direction. Cirino et al. [27] found that sliding parallel to the orientation of fibers yielded a lower wear rate in all the different configurations studied, i.e. carbon/epoxy, glass/epoxy, aramid/epoxy, aramid/PEEK, glass/PEEK and carbon/PEEK. In the present work, CF reinforced laminates exhibited the lowest value of coefficient of friction; this behavior was expected as the carbon creates a solid lubricant phase which acts as a third body between the surfaces.

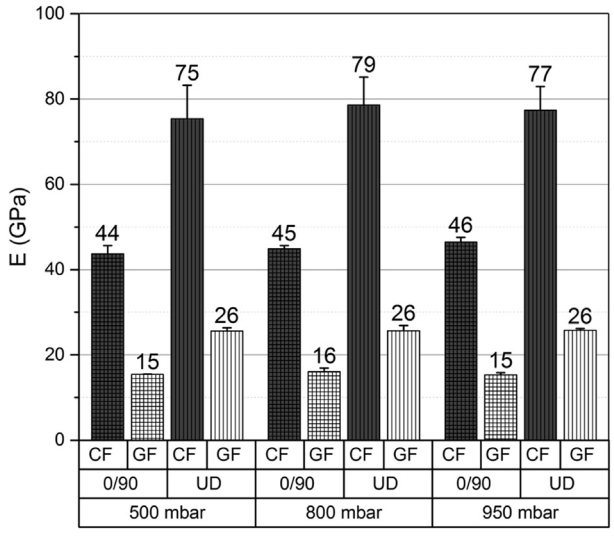

Fig. 5. Tensile modulus of elasticity.

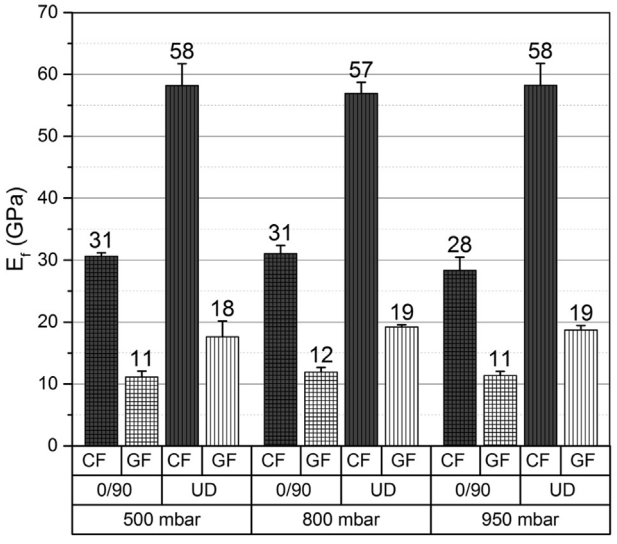

Fig. 7. Flexural modulus of elasticity.

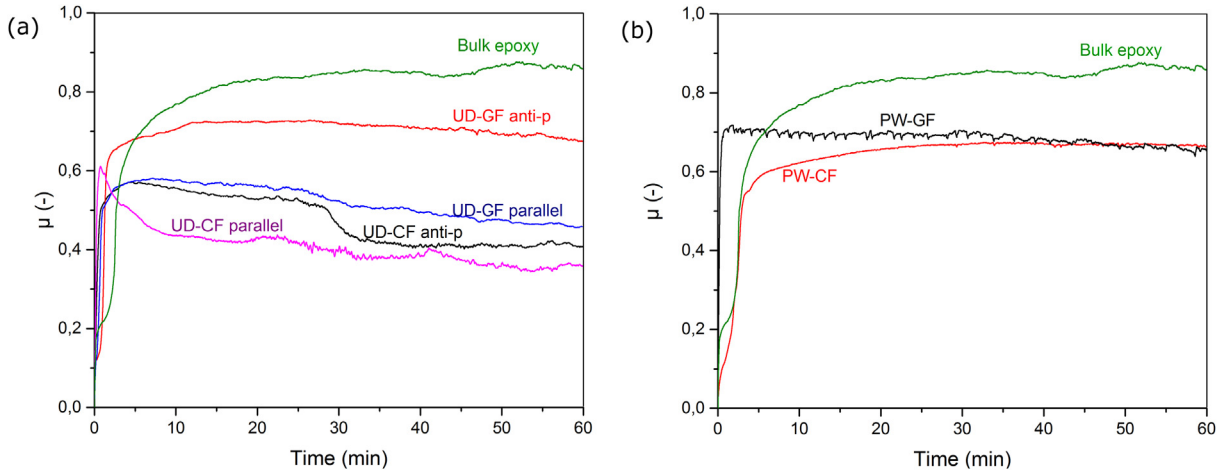

Fig. 8. Comparison of μ curves, in the first 60 min, for epoxy resin and reinforced laminates: (a) UD FRP sliding parallel and anti-parallel, (b) PW FRP.

The analysis of the instantaneous variation of the tangential force during the tests allowed the investigation of the frictional force evolution as function of displacement and time. As an illustrative case, Fig. 10 provides the loop cycles of the frictional force for a UD-GF specimen during sliding of the sphere in anti-parallel direction. Four exemplificative time intervals (beginning, intermediate and final) were selected to illustrate the variation in shape and amplitude of the force for the test duration.

In the right top of the graphs of Fig. 10 it is also present the corresponding bi-dimensional image relative to one sliding cycle. Starting from a flattened shape, the cycle evolves to a more irregular one. Once the running-in flat phase is finished, during the intermediate phase, as the sphere is in the bottom dead center, the friction force has a first peak – corresponding to the presence of a static friction coefficient; after this, μ decreases while the sphere slides. Finally, in the top dead center, the friction force has another static phase value.

Lubricated tests, as expected, evidenced a substantial reduction of the μ (see Fig. 9). In the present investigation, the maximum decrease of μ took place in the PW textile reinforced specimens, with a reduction of 80% and 82% for carbon and glass fiber respectively. On the other hand, the smallest difference was found in the CF specimens with test sliding in parallel direction, recording only 35% of μ reduction. El-Tayeb and Gadelrab [14], using a pin-on-ring system, found a decrease of μ and the wear rate from dry to water lubricated conditions of the GF/epoxy sliding against steel, equal to 30–75% and 62–88% respectively. These results contrast the work by Zhang et al. [28], who examined the μ and wear rate of different epoxy-based composites in diesel-lubricated conditions using a block-on-ring apparatus. A significant increment of the μ was declared when lubricant was injected into a PEEK composite/steel tribopair, due to removal of transfer film. The differences founded in this work are explained considering the different tribo-apparatus used.

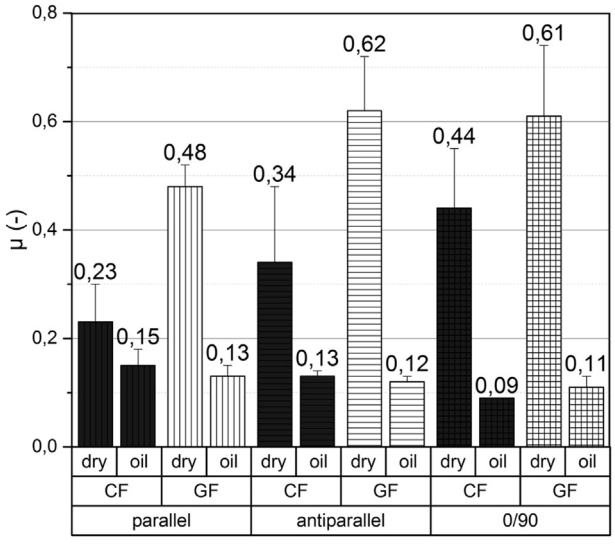

Fig. 9. μ values relative to dry and lubricated (oil) tests.

In Fig. 11 the evolution of the lubricated test for a UD-CF specimen is presented. It shows small changes if compared to the dry test evolution, the same flat running-in phase is evident in the first graph. Afterward the cycle is also irregular, even if milder than the dry one. In Fig. 11 c and d the mean frictional force is higher, this could be attributable to the oil film rupture occurred in the final sliding phase. Moreover, simultaneously to this event, the fiber breakage probably altered the oil film with wear debris.

Topography analysis provided information about the wear phenomena taking place in the system, which completes the tribological behavior in conjunction with the μ [29,30]. As expected, the fracture was more evident when the sliding direction was anti-parallel to the fiber orientation. This statement applies well to both carbon and glass fiber reinforced epoxy. Furthermore, in the UD-CF specimens a presence of voids on the surface was revealed, this presence influenced the wear process, as the fiber were more rapidly exposed to the sliding counterbody. Consequently a relatively lower μ value was measured in specimens where the steel sphere rubbed against an area with a high voids density.

Comparing the topography images of the dry and lubricated tribotest, it was evident a change in the wear depth. Excluding the samples with high voids density on the surface, it was established a peak-to-valley mean value: about 30 μm for the dry test and about 15 μm for lubricated. Furthermore, in the UD samples, the geometry of the scar obtained in lubricated test changed. In the dry tests the worn surface was regular and its deepest values were gained in the midpoint of the sphere stroke. Whereas, in the lubricated tests the worn area was larger and deeper in the bottom and top dead centers (see Fig. 12). This is attributable probably to the instauration of a mixed/hydrodynamic lubrication phenomenon in the center of the stroke, where the steel ball reaches its maximum speed value.

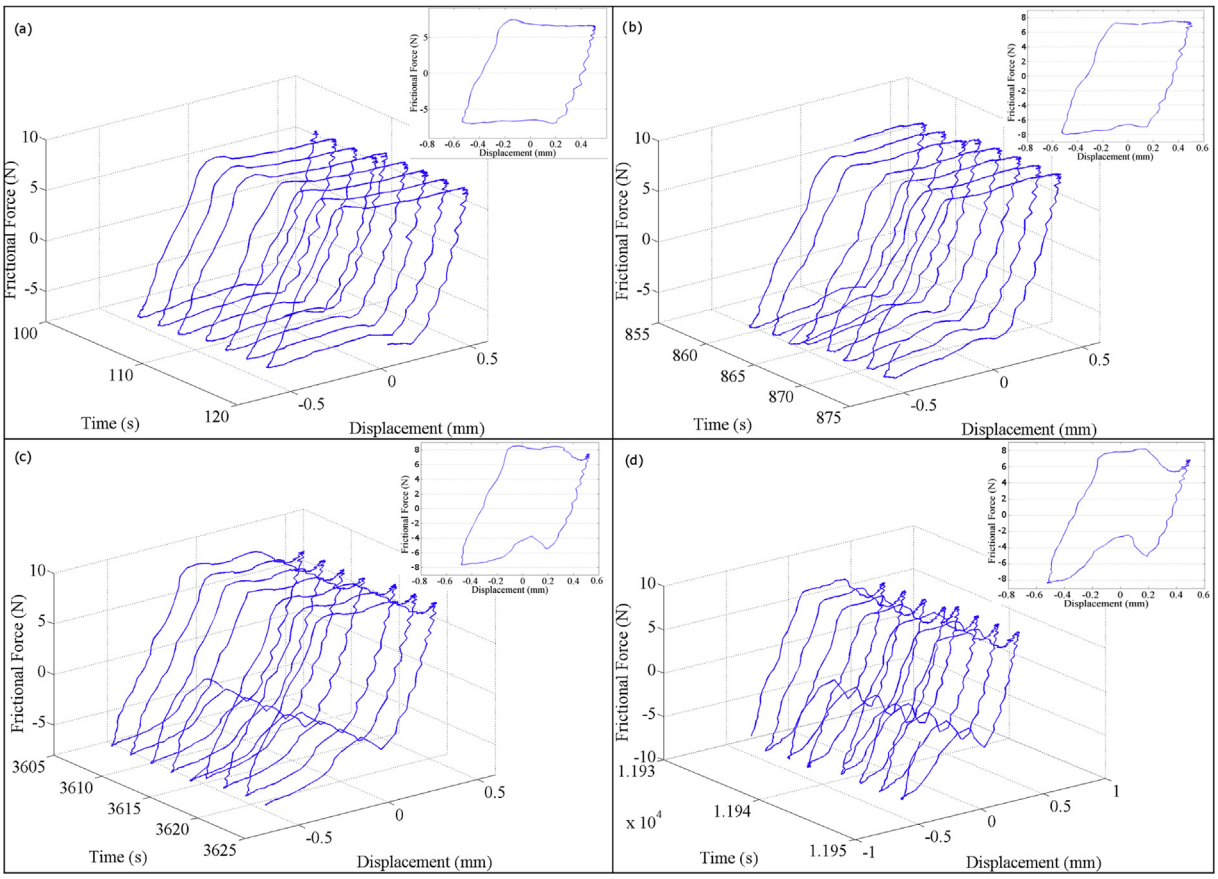

Fig. 10. Evolution of the friction cycle in a dry UD-GF sample sliding in parallel direction. Four time intervals were chosen, (a) beginning, (b and c) intermediate, (d) final phase.

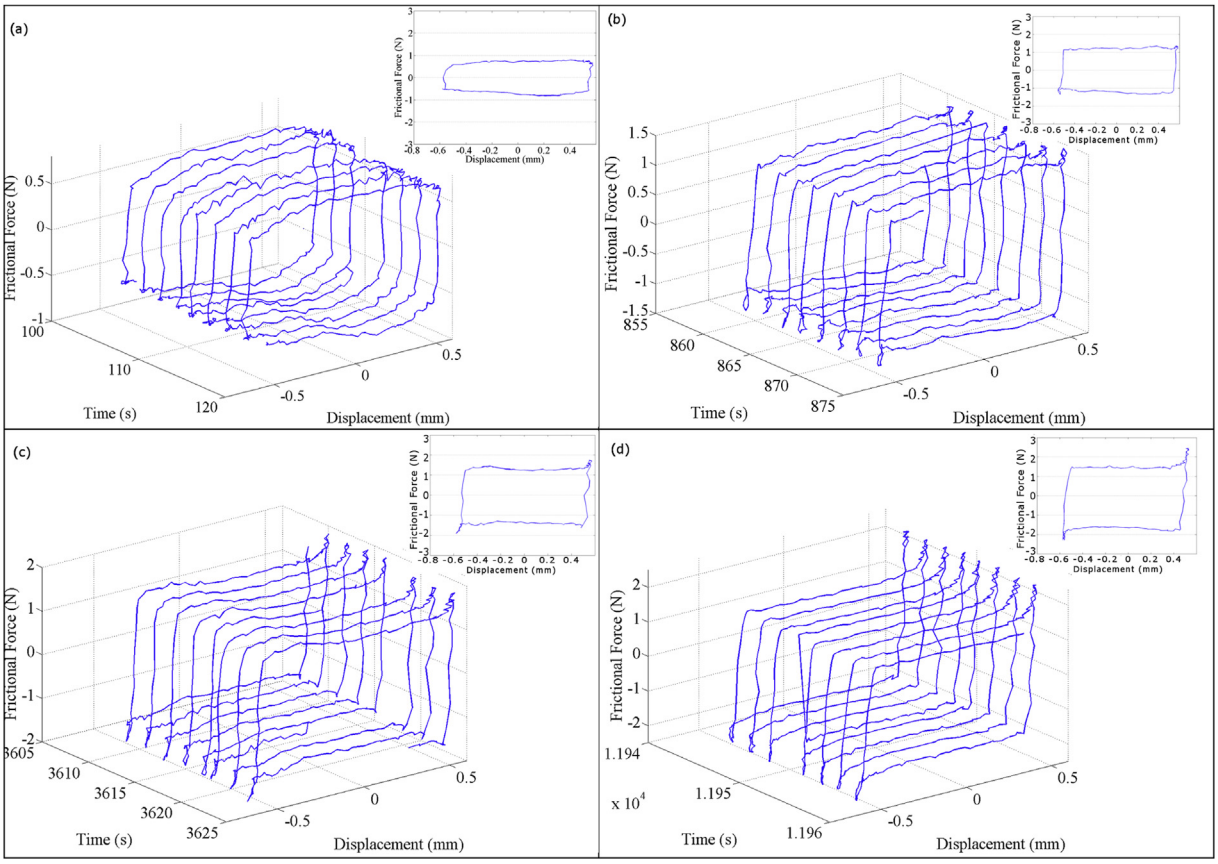

Fig. 11. Evolution of the friction cycle in a lubricated UD-CF sample sliding in parallel direction. Four time intervals were chosen, (a) beginning, (b and c) intermediate, (d) final phase.

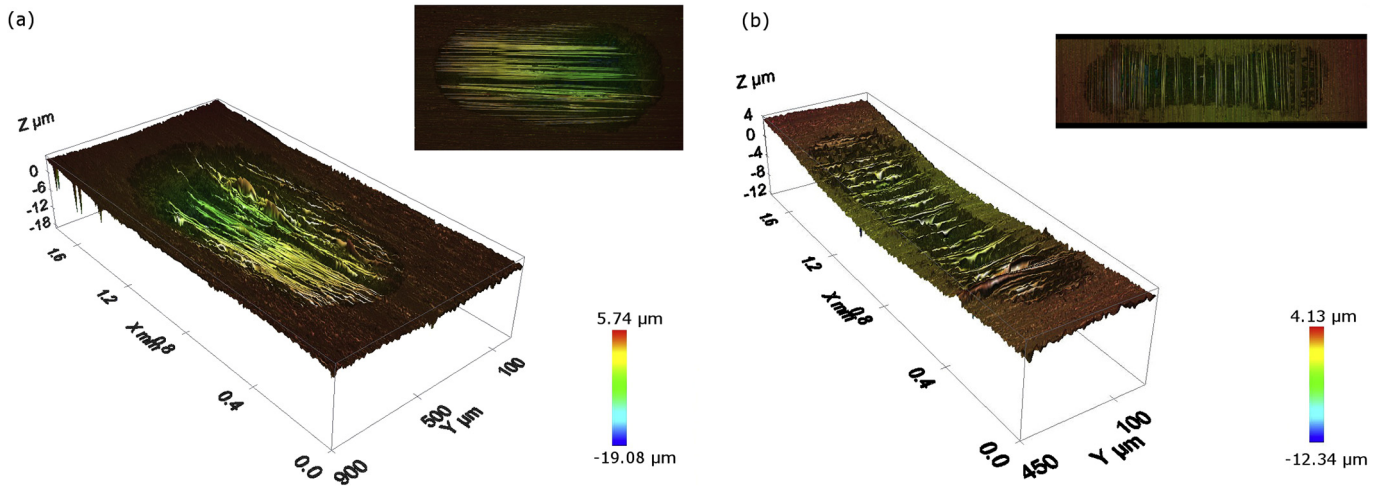

Fig. 12. Wear scar of the CF specimen post tribotest: (a) dry parallel and (b) lubricated anti-parallel.

4. Conclusions

This study investigated twelve glass and carbon FRP composite plates obtained by VARTM, under several aspects: section quality, mechanical properties, dry and lubricated tribo-behavior. A simultaneous presence of both micro and macro voids in the case of low impregnation velocity process has been found, contradicting the theoretical hypothesis of a mutual exclusion. Furthermore, the analysis evidenced how the impregnation quality of composites laminates obtained by VARTM can be considered less afflicted by the impregnation velocity than those obtained by other LCM. The response to the tensile and bending loads was highly influenced by the reinforcement material and its textile geometry rather than by the void volume ratio.

The dry tribotests confirmed the expected behavior, as the presence of fibers inside the epoxy resin lower the μ value. Furthermore, carbon fiber reinforced laminates exhibited the lower coefficient of friction, and sliding parallel to fiber direction lowered the μ in both unidirectional GF and CF. The introduction of film fluid between the sliding surfaces yielded a reduction of μ – about 60% and 80% for CF and GF respectively – whereas it is observed a modification of the wear phenomena along the track. Moreover, when the oil is interposed between the contact surfaces the wear is more severe in the dead centers; and the non-continuous oil injection is responsible for the film rupture and the μ increase during final phases of lubricated test time. Further studies should be made to investigate the phenomenon in analytic way, both to predict the wear process and the quantity of wear debris in FRP composite materials, both to model, in lubricated way, the mechanism of fluid film creation.

Acknowledgments

We gratefully acknowledge Dimitrios Kastanis, University of Leoben, for useful assistance in the laminates production and discussion of results.

References

[1] Friedrich K, Chang L, Haupert F. Current and future applications of polymer composites in the field of tribology. In: Nicolais L, Meo M, Milella E, editors. Composite materials. London: Springer; 2011. p. 129–67.
[2] Valášek P, Müller M, Ružbarský J. Using recycled rubber particles as filler of polymers. Appl Mech Mater 2014;616:260–7.
[3] Valášek P, Müller M. Polymeric particle composites with filler saturated matrix. Manuf Technol 2012;12(13):272–6.
[4] Jaber SA, Ruggiero A, Battaglia S, Affatato S. On the roughness measurement on knee prostheses. Int J Artif Organs 2015;38(1):39–44.
[5] Larsen TO, Andersen TL, Thorning B, Horsewell A, Vigild ME. Comparison of friction and wear for an epoxy resin reinforced by a glass or a carbon/aramid hybrid weave. Wear 2007;262:1013–20.
[6] Ghiorse SR. Effect of void content on the mechanical properties of carbon/epoxy laminates. SAMPE J 1993;24:54–9.
[7] Patel N, Lee LJ. Modeling of void formation and removal in liquid composite molding. part i: wettability analysis. Polym Compos 1996;17(1):96–103.
[8] Patel N, Lee LJ. Modeling of void formation and removal in liquid composite molding. part ii: model development and implementation. Polym Compos 1996;17(1):104–14.
[9] Labat L, Bréard J, Pillut-Lesavre S, Bouquet G. Void fraction prevision in lcm parts. Eur Phys J Appl Phys 2001;16:157–64.
[10] Carlone P, Palazzo GS. Unsaturated and saturated flow front tracking in liquid composite molding processes using dielectric sensors. Appl Compos Mater 2014:1–15.
[11] Lancaster JK. The effect of carbon fibre reinforcement on the friction and wear of polymers. J Phys D Appl Phys 1968;1(5):549–60.
[12] Pihtili H, Tosun N. Effect of load and speed on the wear behaviour of woven glass fabrics and aramid fibre-reinforced composites. Wear 2002;252(11–12):979–84.
[13] Pihtili H. An experimental investigation of wear of glass fibre-epoxy resin and glass fibre-polyester resin composite materials. Eur Polym J 2009;45(1):149–54.
[14] El-Tayeb N, Gadelrab R. Friction and wear properties of e-glass fiber reinforced epoxy composites under different sliding contact conditions. Wear 1996;192:112–7.
[15] Sharma M, Rao I, Bijwe J. Influence of orientation of long fibers in carbon fiber-polyetherimide composites on mechanical and tribological properties. Wear 2009;267:839–45.
[16] Kim SS, Shin MW, Jang H. Tribological properties of short glass fiber reinforced polyamide 12 sliding on medium carbon steel. Wear 2012;274–275:34–42.
[17] Schön J. Coefficient of friction and wear of a carbon fiber epoxy matrix composite. Wear 2004;257:395–407.
[18] Klingshirn C, Koizumi M, Haupert F, Giertzsch H, Friedrich K. Structure and wear of centrifuged epoxy-resin/carbon fiber functionally graded materials. J Mater Sci Lett 2000;19(3):263–6.
[19] Mathew M, Padaki NV, Alagirusamy R, Deopura B, Fangueiro R, Rocha L, et al. Tribological behaviour of multilayered textile composites: the effect of reciprocating sliding frequency. Wear 2009;267:26–33.
[20] Yee RY, Stephens TS. A tga technique for determining graphite fiber content in epoxy composites. Thermochim Acta 1996;272(0):191–9.
[21] Dhieb H, Buijnsters J, Eddoumy F, Celis J. Surface damage of unidirectional carbon fiber reinforced epoxy composites under reciprocating sliding in ambient air. Compos Sci Technol 2011;71:1769–76.
[22] Valášek P, Müller M. Abrasion of polymeric composites on basis of machining splinters from hardfacing alloys - usable in agrocomplex. Acta Univ Agric Silvic Mendel Brun 2014;62(13):261–6.
[23] Hreha P, Radvanská A, Lehocká JCD, Monková K, Krolczyk G, Ruggiero A, et al. Monitoring of focusing tube wear during abrasive waterjet (awj) cutting of aisi 309. Metalurgija 2014;53(4):533–6.
[24] Hloch S, Valíček J. Topographical anomaly on surfaces created by abrasive waterjet. Int J Adv Manuf Tech 2012;59(5–8):593–604.

[25] Zhu HY, Li DH, Zhang DX, Wu BC, Chen YY. Influence of voids on interlaminar shear strength of carbon/epoxy fabric lamiantes. Trans Nonferrous Met Soc China 2009;19:470–5.
[26] Merola M, Carlone P, Ruggiero A, Archodoulaki VM. Mechanical and tribological characterization of composite laminates manufactured by liquid composite molding processes. Key Eng Mater 2015:651–3. In press.
[27] Cirino M, Friedrich K, Pipes RB. Evaluation of polymer composites for sliding and abrasive wear applications. Composites 1988;19(5):383–92.
[28] Zhang G, Burkhart T, Wetzel B. Tribological behavior of epoxy composites under diesel-lubricated conditions. Wear 2013;307(1–2):174–81.
[29] Valicek J, Hloch S. Optical measurement of surface and topographical parameters investigation created by abrasive waterjet. Int J Surf Sci Eng 2009;3:360–73.
[30] Valicek J, Hloch S. Estimation of the smooth zone maximal depth at surfaces created by abrasive waterjet. Int J Surf Sci Eng 2009;3:360–73.